



# Damage Prediction of Integrated Composite T-Joint with Fixed Support Subjected to Low-Velocity Impact: An Experimental and Numerical Study

Rujian Zhu<sup>1</sup> · Xiwu Xu<sup>1</sup> · Chunjian Mao<sup>1</sup>

Received: 13 August 2018 / Accepted: 1 November 2018 / Published online: 2 January 2019  
© The Korean Society for Aeronautical & Space Sciences and Springer Nature Singapore Pte Ltd. 2019

## Abstract

A finite element model was established based on Hashin failure criteria and the progressive damage theory to predict the damage of integrated composite T-joint structures with fixed support subjected to low-velocity impact. The cohesive zone model was employed to simulate the delamination behaviors of adhesive in the finite element model. The fiber damage and matrix damage of each ply can be provided by the finite element model in details. The damage behaviors of composite T-joint structure subjected to different impact energies were compared using the finite element model. The numerical results showed that the impact caused an elliptical projected area with its major axis along the surface fiber direction. Besides, the in-plane damage dimension is proportional to the impact energy. It is obviously noted that the damage of the first ply is the most serious owing to the delamination between soleplate and fillet caused by the stretching of the L-ribs. A low-velocity impact experiment of composite T-joint was also conducted and the damage dimension was determined by the ultrasonic C-scan. Results showed that the shape and size of our experimental damage agreed well with the simulation results. Our finite element model can be used to effectively analyze the damage behaviors of the integrated composite T-joint subjected to low-velocity impact.

**Keywords** T-joint · Finite element model · Low-velocity impact · Impact damage

## 1 Introduction

Composite structures are widely used in aerospace, automotive and other high-performance applications owing to its high specific strength, high specific stiffness and designable [1–4]. However, composite structures are sensitive to impact damage [5–7] and it may cause the decrease of structure strength because of the fragile property, which is a critical disadvantage for their application in aircrafts. During the service life of aircraft, impact damage is easily occurred by different situations, such as impact of small objects, such as hailstones, runway debris or falling tools [8]. In all impact issues, barely visible impact damage (BVID) [9] is one of the most common cases and hence the issue about composite structures with BVID has attached great interest to aircraft

designers [10]. Integrated composite T-joint is a typical unit of aircraft structures, which can be used as not only a rib to increase strength and stiffness of skins, but also a part of vertical and horizontal panels to transfer loadings from other parts. Therefore, it is important to study in detail the impact phenomenon of composite T-joint.

To explore the damage behaviors of composite structures under impact conditions, many investigations [11–13] have been implemented in the past decades. Wang [14] investigated low-velocity impact characteristics of carbon fiber composite laminates after impact by means of numerical and experimental methods. The finite element model was created using a subroutine to enhance the damage simulation through the use of Hashin and Yeh failure criteria. Besant [15] predicted the behaviors of composite sandwich panels under low-velocity impact by finite element analysis, brick elements were employed for the honey comb core and shell elements are applied for the carbon/epoxy skins. The numerical and experimental study on low-velocity impact problem of electrospun nanofiber-modified composite laminates is proposed by Hesam Yademellat [16]. The results reveal that

✉ Xiwu Xu  
nuaaxuxiwu@126.com

<sup>1</sup> The State Key Laboratory of Mechanics and Control of Mechanical Structures, Nanjing University of Aeronautics and Astronautics, Nanjing 210016, People's Republic of China

the damage caused by the impact loading is reduced by the interleaving nanofiber mats between the layers of the composite laminate, typically the size of the delamination.

The structures having T-joints are often subjected to tension, bending, flexure and out-of-plane shear loading [17–20]. In recent years, many scholars have done analyses of the low-velocity impact damage of stiffened plates [21–23]. Benjamin Ostre [24] carried out a finite element analysis of low-velocity energy edge impact on carbon fiber-reinforced plastic T-joint. This edge impact model employs out-of-plan impact model on a laminate plate with new friction and crushing behavior, which corresponds with force–time and force–displacement curves, damage morphology and permanent indentation after impact. However, the fiber failure in compression was not considered in the model. Faggiani [25] developed a damage model based on a continuum damage mechanics to analyze the damage mechanisms occurred in carbon fiber composite structures, and the mechanisms included fiber tensile and compressive breakage, matrix tensile and compressive fracture, and shear failure. Friction and contact algorithms between delaminated laminates were conducted to better simulate the impact event. Greenhalgh [26] had analyzed the damage in different positions of the skin–stringer composite structures. Yu Feng [27] studied the effect of impact damage positions on the damage behaviors of stiffened composite panels. The results revealed that the thickness of the impact position had an influence on the impact crater depth. The failure loads of damaged specimens were related to different impact positions. Serna Moreno [28] optimised the geometry of the adhesive to increase the amount of energy dissipated owing to the damage of the

adhesive during the impact. They studied the behavior of a bonded joint of two composites subjected to impact loading by the finite element method. For the research mentioned above, low-velocity impact of integrated composite T-joint with fixed support has been concerned little, so the issue was studied in this paper.

A 3D dynamic finite element model was proposed using ABAQUS software to predict the progressive damage of integrated composite T-joint laminates subjected to low-velocity impact with fixed support; a VUMAT subroutine was developed to analyze the damage of the fiber and matrix after the impact. Experimental results and finite element model analysis are presented in the following sections.

## 2 Description of Experimental Program

### 2.1 Preparations of Composite T-Joint

T700/QY9611 unidirectional prepreg, provided by Chengdu aircraft design and Research Institute of China Aviation Industry, was used for T-joint in this paper. T700 is 3 k carbon fiber produced by Toray Industry, Inc. and QY9611 is a native bismaleimide resin in China. The main parameters of T700/QY9611 composites are shown in Table 1.

The T-joint specimen is composed of two L-ribs (sublaminates-1, sublaminates-2), a triangle filling zone (fillet), and a soleplate (sublaminates-3). The L-rib includes a vertical component (center plate), a curved component, and a horizontal flange (over-laminate) bonded with the soleplate, as shown in Fig. 1.

**Table 1** Mechanical property of T700/QY9611

Parameter	$E_{11}$ (GPa)	$E_{22}$ (GPa)	$\mu_{12}$	$G_{12}$ (MPa)	$X_t$ (MPa)
Value	131	10.6	0.27	6.03	2920
Parameter	$X_c$ (MPa)	$Y_t$ (MPa)	$Y_c$ (MPa)	$G_{Ic}$ ( $J \times m^{-2}$ )	$G_{IIc}$ ( $J \times m^{-2}$ )
Value	1392	62.8	240	642	748

**Fig. 1** Schematic diagram of the composite T-joint structure; **a** dimension of T-joint; **b** components of T-joint

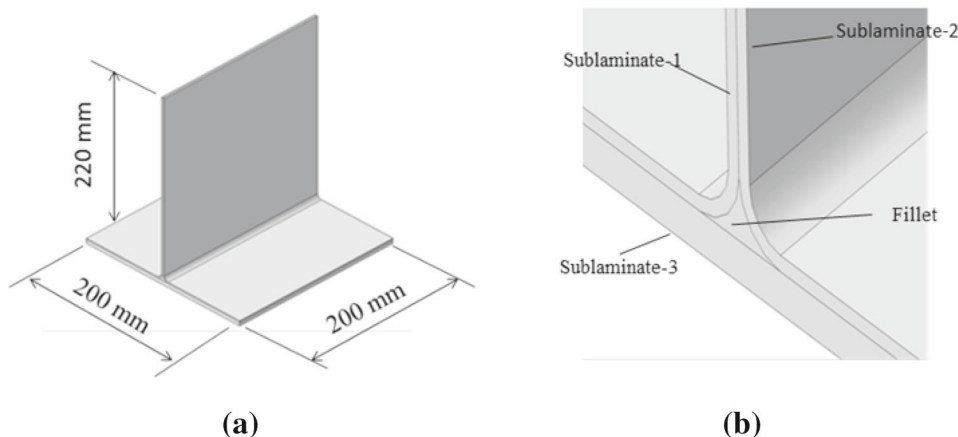
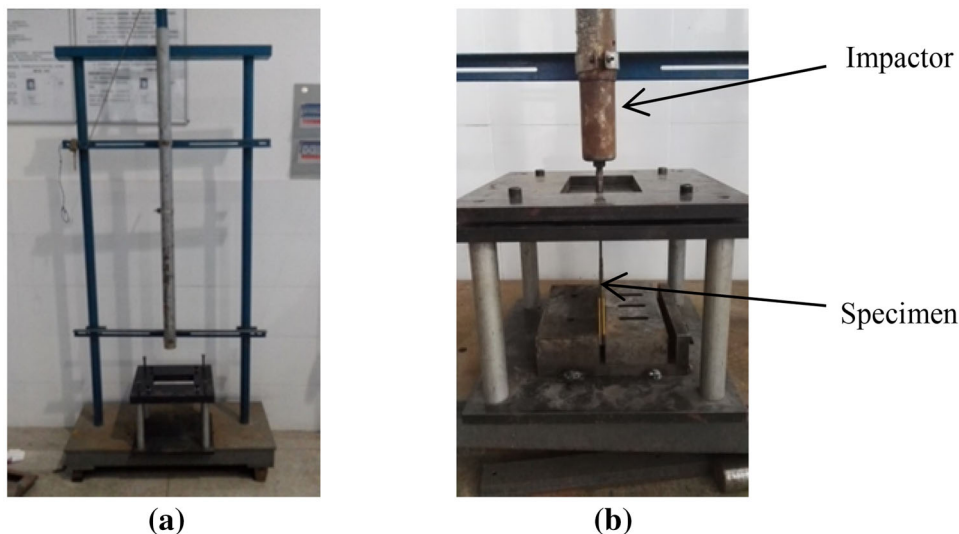


**Fig. 2** Test setup **a** impact setup; **b** impact support fixture



Thicknesses of sublaminates-1 and sublaminates-2 are both 1.75 mm, with layup sequence of [45/-45/90/0/45/90/-45/0/-45/45/90/0/45/-45] from outside to inside. Thickness of sublaminates-3 is 4.5 mm, with layup sequence of [45/0/-45/90/45/0/45/0/45/-45/0/45/0/-45/45/0/-45/0]s. The fillet among the soleplate and two L-ribs was filled with prepreg according to the volume of the gap in the trigone, whose radius bend  $R$  in the fillet region is 5 mm.

To ensure the integrity of the structure, a co-bonding process was adopted. The two L-ribs, the fillet and the soleplate were assembled, bagged up and vacuumed for an autoclave curing cycles. Before the test, the specimens were numbered by AA-1, AA-2 and AA-3 for low-velocity impact test of 8.90 J/mm impact energy, and by AA-4, AA-5 and AA-6 for low-velocity impact test of 4.45 J/mm impact energy.

## 2.2 Test Setup and Procedures

Specimens were examined by ultrasonic C-scan to ensure that there is no existence of initial internal damage in the inner laminate before the impact experiment. A drop tower was used to conduct the impact tests in this study as shown in Fig. 2a. The test specimens were subjected to a concentrated impact using a 16-mm-diameter hemispherical striker with 5.5 kg of total weight from various heights. The impact energy required for evaluating the damage resistance of composite materials is governed from the following equation:

$$E = C_E h, \quad (1)$$

where  $E$  is the potential energy of impactor prior to drop,  $C_E$  is the specified ratio of impact energy to specimen thickness, 4.45 J/mm or 8.90 J/mm, and  $h$  is the nominal thickness of the specimen. Utilizing Eq. (1), the impact energy of 27.81 J and 55.62 J was calculated for the composite testing. The impact

velocities and drop heights of the two chosen energy levels were 3.18 m/s and 4.50 m/s, and 516 mm and 1032 mm, respectively. Three specimens were tested for each energy level to determine repeatability of the test experiment. During the test, the specimen was placed centered relative to the cutout (200 mm × 120 mm) and was fixed on the impact support fixture as shown in Fig. 2b by adjusting the tightness of the bolt during the experiment. To prevent the second impact during the test, a stick was inserted artificially to isolate the specimen and the impactor after the rebound of the impactor. The inner damage dimension of the specimens was detected by ultrasonic C-scan and the impact crater depth after the impact test was determined using the depth micrometer.

## 2.3 Experimental Results and Discussion

A total number of six specimens were tested at two different energy levels for investigating the impact behavior of T-joint with fix support. Figure 3 illustrates the detail photographs of surface damage after impact. As shown in Fig. 3a, there is a visible indentation caused by the impact energy of 4.45 J/mm in the laminate surface; however, it is obviously noted that the impact caused serious damage in the laminate surface at the impact energy of 8.90 J/mm with fiber cracks and matrix cracks as shown in Fig. 3b. The fiber direction determines the direction of the damage and the crater depth of specimens is given in Table 2. Naturally, the crater depth of T-joint subjected to the impact energy of 8.90 J/mm were much deeper than 4.45 J/mm. Figure 3c, d shows the result of the ultrasonic C-scanning after impact, and a visible ellipse can be observed in the central of the specimen with its major axis along the fiber direction of the surface ply. The damage area of the ultrasonic C-scanning is the combination of the delamination and laminate ply damage; different colors in the ellipse represent the damage caused by the impact in the

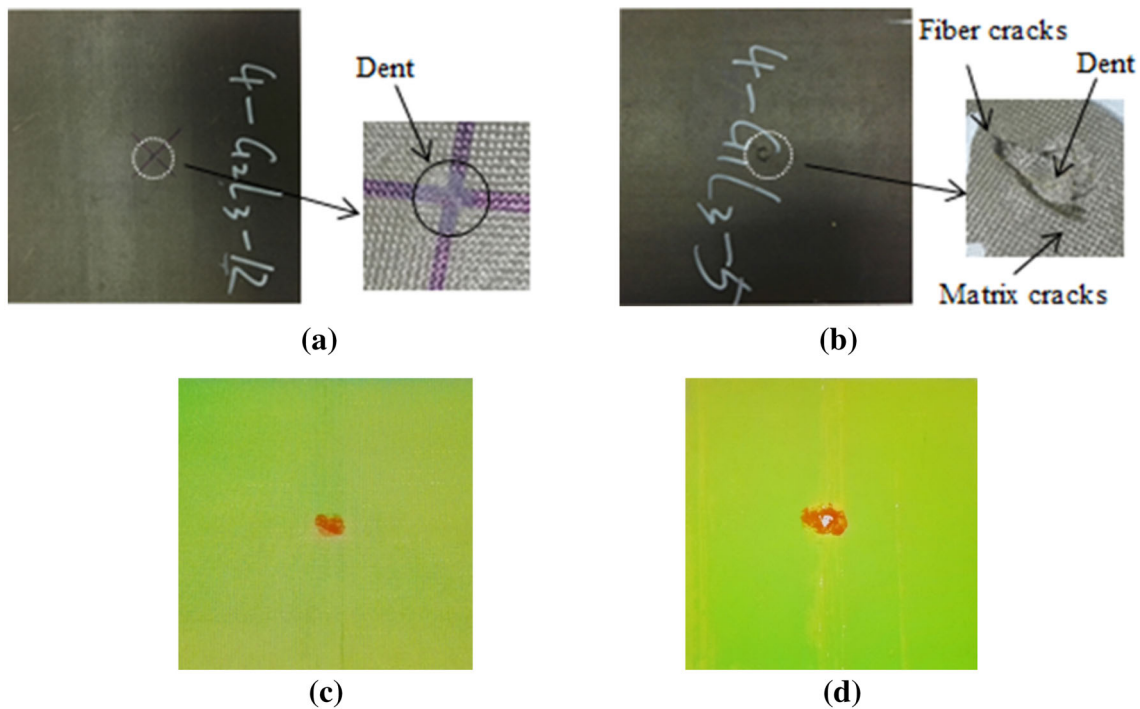


**Fig. 3** Direct observation and ultrasonic C-scan results of the damage of composite T-joint impacted at different energies **a** 4.45 J/mm; **b** 8.90 J/mm; **c** 4.45 J/mm; **d** 8.90 J/mm

**Table 2** Comparison of crater depth of specimens

Label	AA-1	AA-2	AA-3	AA-4	AA-5	AA-6
Depth (mm)	0.775	0.815	0.705	0.115	0.135	0.185

different laminate layer. Naturally, the higher impact energy can result in the more serious damage according to the result of the ultrasonic C-scan.

### 3 Numerical Study

#### 3.1 Finite Element Model

The experimental results can only provide the projected damage area and depth of whole composite T-joint structure quantitatively and qualitatively as shown in Fig. 3, while the damage behaviors of every fiber layer and matrix layer cannot be provided by above-mentioned experimental analysis. In [29], they once established finite element model to analyze the damage behaviors of every fiber layer and matrix layer in their fiber reinforced composite laminate in details. Therefore, for our composite T-joint structure in Fig. 1, a non-linear finite element model was developed using progressive damage model to simulate the impact behavior in the commercial software ABAQUS/Explicit.

Schematic diagram of composite T-joint structure subjected to low-velocity impact is shown in Fig. 4. The

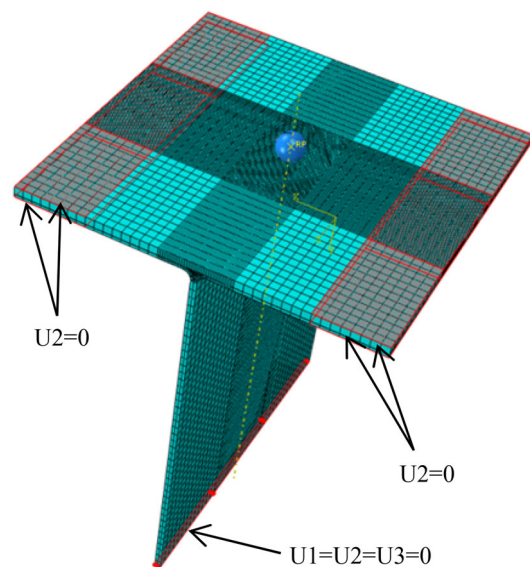


**Fig. 4** Assembled FE model with boundary conditions

impactor was modeled by an analytical rigid ball. Since the delamination is prone to occur at the interface between different components, an eight-node three-dimensional cohesive

element (COH3D8) was modeled between sublaminates-1, sublaminates-2 and sublaminates-3, which has a thickness of 0.01 mm, one-tenth of the single laminate thickness. All layers of composite were modeled using eight-node quadrilateral in-plane general-purpose continuum shell element (SC8R). The fillet was filled with isotropy resin which was modeled using eight-node linear brick reduced integration element (C3D8R). The mesh density around the impact point was chosen as 1 mm × 1 mm on the basis of mesh sensitivity analysis in terms of computational time and convergence solution, and the others are 1 mm × 5 mm and 5 mm × 5 mm, respectively. A mass of 5.5 kg was assigned to the impactor, matching the experimental test conditions. Different initial impact velocities were imposed to the impactor to simulate different impact energy level events. The upper and lower surfaces of the left and right edges in Fig. 4 were fixed, which have a length of 40 mm. Besides, the bottom edge of L-ribs is also fixed as the boundary condition. Freedom of the impact is limited except the impact direction. The interaction between the specimen and impactor was simulated by surface to surface contact and the mechanical constraint formulation was enforced using the kinematic contact algorithm.

## 3.2 Failure Analysis

### 3.2.1 In-Plane Damage Initiation Criteria

The material failure in plane is complex, which consists of fiber cracking, fiber crushing, matrix cracking and matrix crushing. The strain-based Hashin criteria [30] were employed to determine the inter-laminar damages in this paper. Each of the damage modes is predicted by the following expressions: fiber cracking  $\varepsilon_{11} \geq 0$ :

$$\left(\frac{\varepsilon_{11}}{\varepsilon_{11}^t}\right)^2 + \left(\frac{\varepsilon_{12}}{\gamma_{12}}\right)^2 \geq 1, \quad (2)$$

fiber crushing  $\varepsilon_{11} < 0$ :

$$\left(\frac{-\varepsilon_{11}}{\varepsilon_{11}^c}\right)^2 \geq 1, \quad (3)$$

matrix cracking  $\varepsilon_{22} \geq 0$ :

$$\left(\frac{\varepsilon_{22}}{\varepsilon_{22}^t}\right)^2 + \left(\frac{\varepsilon_{12}}{\gamma_{12}}\right)^2 \geq 1, \quad (4)$$

matrix crushing  $\varepsilon_{22} < 0$ :

$$\left(\frac{E_{22}\varepsilon_{22}}{2G_{12}\gamma_{12}}\right)^2 + \left(\frac{\varepsilon_{22}}{\varepsilon_{22}^c}\right)^2 \left[\left(\frac{E_{22}\varepsilon_{22}^c}{2G_{12}\gamma_{12}}\right)^2 - 1\right] + \left(\frac{\varepsilon_{12}}{\gamma_{12}}\right)^2 \geq 1, \quad (5)$$

**Table 3** Material property degradation rules

Damage mode	Property degradation rule
Fiber cracking	$E'_{11} = 0.07E_{11}$
Fiber crushing	$E'_{11} = 0.14E_{11}$
Matrix cracking	$E'_{22} = 0.2E_{22}, G'_{12} = 0.2G_{12}, G'_{23} = 0.2G_{23}$
Matrix crushing	$E'_{22} = 0.4E_{22}, G'_{12} = 0.4G_{12}, G'_{23} = 0.4G_{23}$

where  $\varepsilon_{11}^t$  and  $\varepsilon_{11}^c$  are the tensile failure strain and compress failure strain referring to a local coordinate system;  $\varepsilon_{22}^t$  and  $\varepsilon_{22}^c$  represent the tensile failure strain and compress failure strain in the transverse direction;  $\gamma_{12}$  is the shear failure strain in plane, and  $E_{11}$  and  $E_{22}$  represent the elastic modulus in the coordinate system;  $G_{12}$  is the shear modulus, respectively. As long as the stress components within a specific layer of an element satisfy the failure criterion, the corresponding damage mode will occur.

### 3.2.2 Property Degradation

Once damage occurs, the material constants in every layer of the laminate should be modified. The degradation technique proposed by Camanho [31] supposed that the effect of damage on the material constants can be represented using internal state variable. This approach is widely used because it can adjust the value of the internal state variables in accordance with the predicted type of different failure modes, which is a more suitable simulation of damage accumulation. The property degradation rules are shown in Table 3.

### 3.2.3 Cohesive Model for Delamination

An inter-laminar damage model is demanded for the simulation of impact to model the initiation and propagation of delamination between different components in the composite laminate. A traction–separation model based on damage mechanics, which includes an initially linear elastic behavior together with the initiation and evolution of damage, was employed for this study [32]. Figure 5 shows the relationship between equivalent stress and strain of the cohesive. The stress–strain curve shows a linear elastic stage before the load achieves the critical value at point A. Whether a stress limit is reached is decided based on damage initiation criteria. Once the normal or shear tractions reach their inter-laminar tensile and shear strengths, respectively, the stiffness of the cohesive element reduced gradually to zero from point A to point C; point C represents a complete failure of materials [33–35]. Unloading of the cohesive element, for example, at point B,

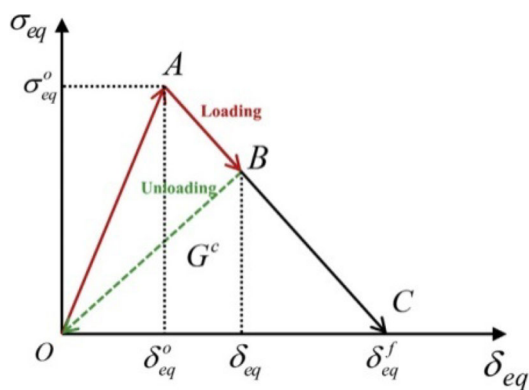


Fig. 5 Relationship between equivalent stress and strain of cohesive

the stress reduced from point B towards the origin, which forms a new stress–strain curve.

The initiation of delamination damage is estimated using the quadratic nominal stress criterion defined by the following expression:

$$\left(\frac{t_n}{N}\right)^2 + \left(\frac{t_s}{S}\right)^2 + \left(\frac{t_t}{T}\right)^2 = 1, \tag{6}$$

where  $t_n$  is the inter-laminate normal tensile stress, and  $t_s$  and  $t_t$  are shear stresses in the two transverse directions.  $N$ ,  $S$  and  $T$  represent the normal tensile strength and shear strengths, respectively.

For mixed-mode damage initiation and propagation, a Benzeggagh–Kenane (BK) fracture energy-based criterion was used to simulate mixed-mode inter-laminar damage evolution. It is given by the following expression:

$$\left(\frac{G_I}{G_{IC}}\right)^2 + \left(\frac{G_{II}}{G_{IIC}}\right)^2 + \left(\frac{G_{III}}{G_{IIIC}}\right)^2 = 1, \tag{7}$$

where  $G_{IC}$  is the normal strain energy release rate, and  $G_{IIC}$  and  $G_{IIIC}$  are shear strain energy release rates in the two transverse directions. The property parameters of cohesive element provided by Chengdu aircraft design and Research Institute of China Aviation Industry are given in Table 4.

### 3.2.4 Flowchart of the Model

Based on the proposed numerical model, a parametric modeling program has been developed to predict the impact damage process. The flowchart is shown in Fig. 6. The left part of the

figure represents the flowchart of impact damage analysis, while the right part describes the flowchart of the damage progression subjected to low-velocity impact.

### 3.3 Numerical Results and Discussion

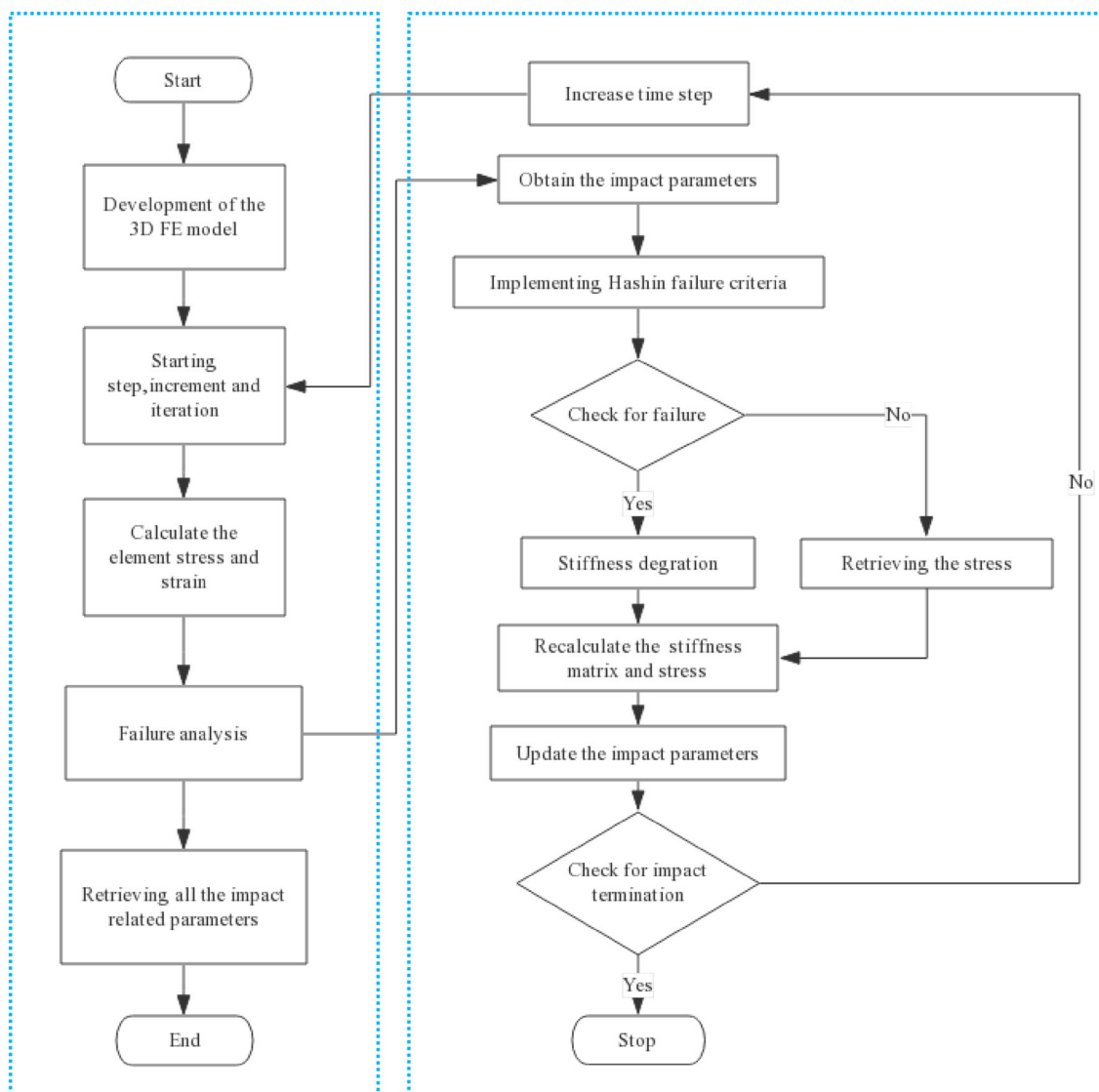
Figure 7 shows the comparison of projected damage area between the experimental and the numerical results (consists of laminate damage and delamination). It can be noticed that the damage projected area at both impact energy look like an ellipse with the major axis along the fiber direction of the surface laminate ply. The higher impact energy caused larger damage area. Table 5 reveals the damage area comparison between numerical result and experimental result. The area errors 3% and 9% are in the error range of the engineering permission. Therefore, the finite element model is reliable to predict the damage characteristics of the composite T-joint structure subjected to low-velocity impact.

Damage area of every laminate ply can be presented in this model. However, in this paper we only provide damage schematics of some typical layers, such as the top four laminate layers, the middle four layers and the bottom four laminate layers in composite sublaminar-3 after the impact as shown in Fig. 8. This is mainly due to the reason that the damage of the top and bottom layers is most serious and the damage of middle layers is similar. The first ply referred to the lamina adjacent to the cohesive and the thirty-sixth ply referred to impacted surface. It is obviously noted that the impact caused larger damage area in the top and bottom laminate layers than middle layers. The damage area shape of the top and bottom laminate layers looks like an ellipse. Besides, the ellipse’s major axis is along the fiber direction with laminate layers adjacent to the cohesive, while the ellipse’s major axis of the laminate layers adjacent to the impact surface is vertical to the fiber direction. Therefore, the damage area shape of the first ply determines the damage projected area which agrees well with Fig. 7.

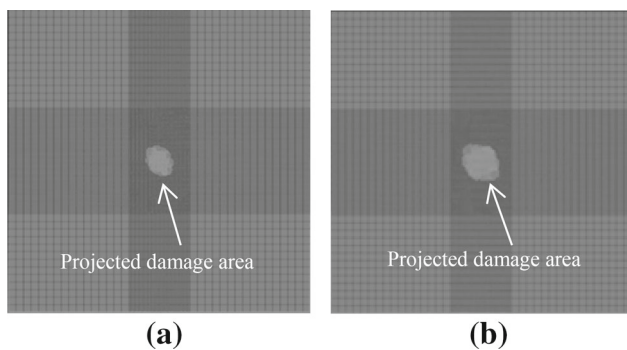
Figure 9 gives the inner-laminar damage of the first ply and thirty-sixth ply with the same fiber direction at the impact energy of 8.90 J/mm, i.e., the damage behaviors of fiber and matrix for a single laminate layer. It can be observed that the damage is caused by the matrix cracking primarily, which led to the different major axis of the ellipse. The final delamination of cohesive element presented by damage variable is usually set above 0.9999. Figure 10 shows the numerical result of cohesive at the impact energy of 4.45 J/mm and 8.90 J/mm. The impact causes two-lobe delamination

Table 4 Property parameters of cohesive

$P$ (kg/m <sup>3</sup> )	$K_n$ (MPa)	$K_s = k_t$ (MPa)	$N$ (MPa)	$T = S$ (MPa)	$G_{IC}$ (J/m <sup>2</sup> )	$G_{IIC} = G_{IIIC}$ (J/m <sup>2</sup> )
1520	1200	600	5	10	642	748



**Fig. 6** Flow chart of VUMAT subroutine and ABAQUS software



**Fig. 7** Comparison of projected damage area subjected to different impact energies, **a** 4.45 J/mm, **b** 8.90 J/mm

at the impact energy of 4.45 J/mm, while the delamination of impact energy of 8.90 J/mm looks like a strip owing to the fact that the delamination progression results from the

stretching of the L-ribs. It can also be observed that the delamination area caused by the impact is smaller than the damage projection area of the laminate, which cannot be seen from the ultrasonic C-scanning. Hence, the finite element model is very useful to understand the damage of inner fiber and matrix.

The numerical damage area of layers in sublaminates-3 is given in Fig. 11. The damage area is in parabolic relation to the laminate ply approximately with the minimum damage area occurring in 25th laminate ply due to the minimum bending of the layer, whose damage area was only 14 mm<sup>2</sup> and 23 mm<sup>2</sup> for the impact energy of 4.45 J/mm and 8.90 J/mm. It is noted that the damage in the first ply is the most serious owing to the delamination. The higher impact energy can result in the faster damage area decreased from ply 1 to ply 25 and increased from ply 25 to ply 36. Figure 12 shows the

**Table 5** Numerical result of delamination compared to experiment results

Label	AA-1	AA-2	AA-3	Average	Simulation	Error (%)
Area (mm <sup>2</sup> )	452	448	464	455	467	3%
Label	AA-4	AA-5	AA-6	Average	Simulation	Error (%)
Area (mm <sup>2</sup> )	198	208	192	199	218	9%

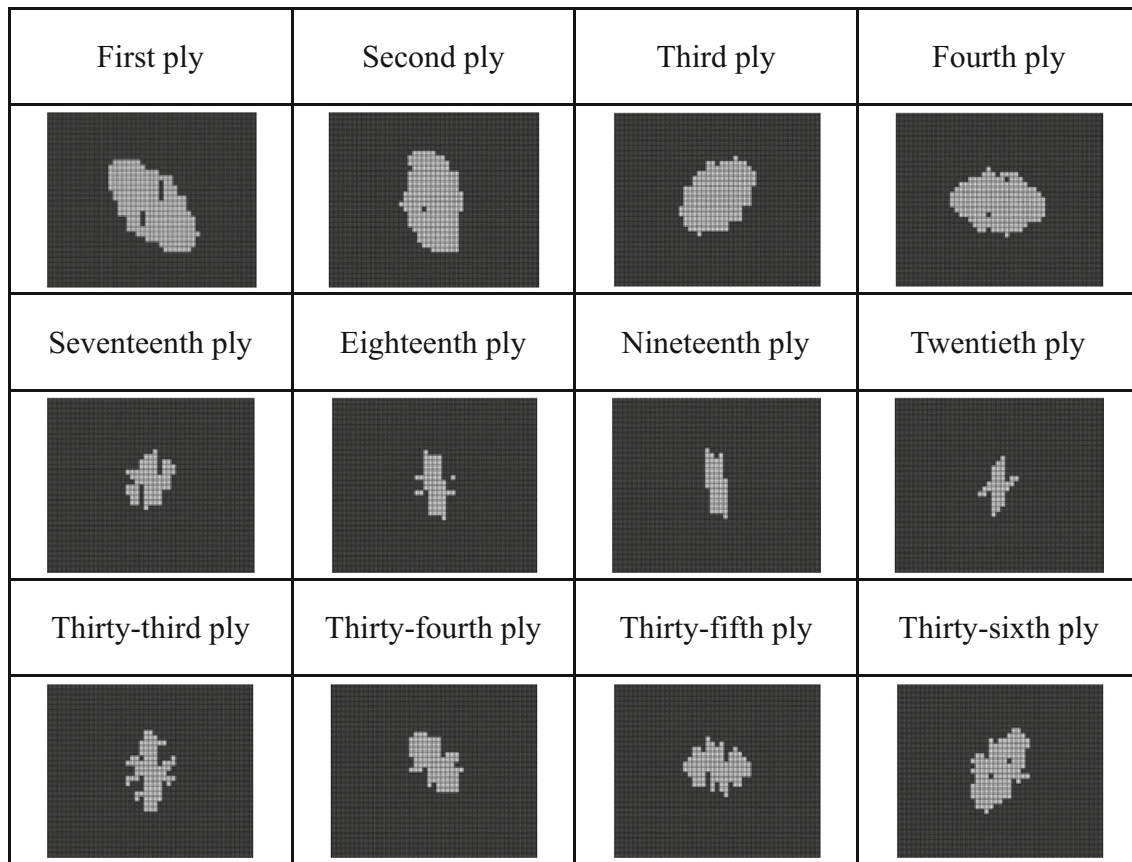


**Fig. 8** The top four laminate layers, the middle four layers and the bottom four laminate layers of damage graph in composite sublaminates-3 after the impact energy of 4.45 J/mm

damage of sublaminates-2 in ply 1, in which damage is more serious than the damage in sublaminates-3. However, it cannot be observed in the surface ply by the experiment for the reason that damage was mainly caused by matrix crushing with little damage in fiber.

### 4 Conclusions

This paper presents the results of experimental and numerical investigations on the impact damage of integrated composite T-joint subjected to low-velocity impact with fixed support. A total number of six specimens were tested using a drop tower test setup for different impact energy levels. The specimens were recorded and the impact damage was detected by ultrasonic C-scan. A 3D dynamic finite element model

was proposed to predict the progressive damage of composite T-joint laminates subjected to low-velocity impact, and numerical results were compared and verified with experimental results. The conclusions are summarized as the following.

The impact with the impact energy of 4.45 J/mm caused a visible dent in the surface, while the impact with larger impact energy of 8.90 J/mm caused visible fiber crushing and matrix cracking. An elliptical projected damage area occurred with its major axis along the fiber direction of the surface laminate ply. The higher impact energy caused larger damage area which can be seen clearly from the result of the ultrasonic C-scan.

The projected damage area predicted by the finite element model agrees well with the experimental results. It is obvious that the damage in the first ply is the most serious owing to the



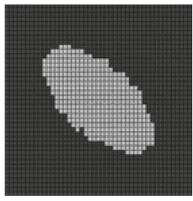
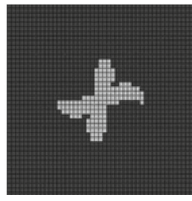
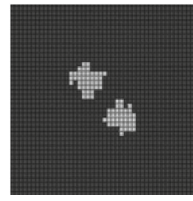
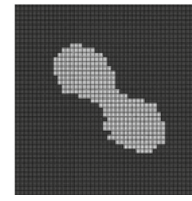
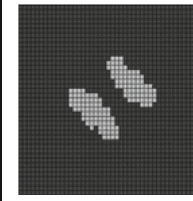
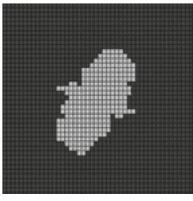
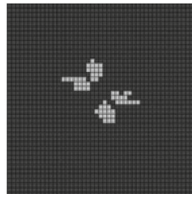
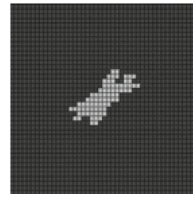
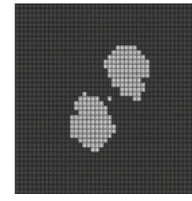
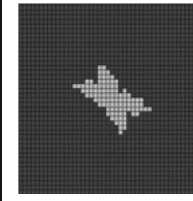
First ply	Fiber cracking	Fiber crushing	Matrix cracking	Matrix crushing
				
Thirty-sixth ply	Fiber cracking	Fiber crushing	Matrix cracking	Matrix crushing
				

Fig. 9 Components of the inter-laminar damage for the first ply and thirty-sixth ply at the impact energy of 8.90 J/mm

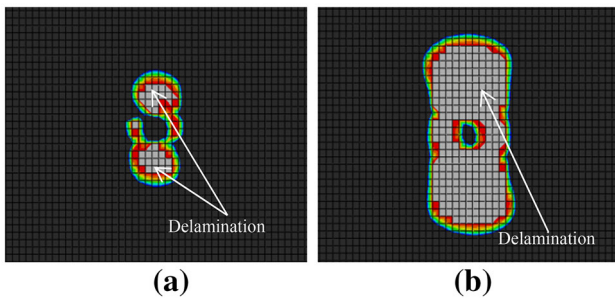


Fig. 10 Details of delamination at the impact energy of a 4.45 J/mm, b 8.90 J/mm

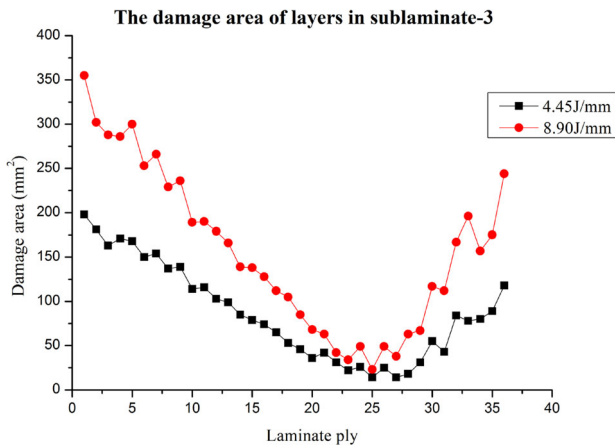


Fig. 11 The damage area of layers in sublaminante-3

delamination, and the delamination progression is due to the stretching of the L-ribs. It is noticed that the minimum damage in sublaminante-3 occurred in 25th laminate ply owing

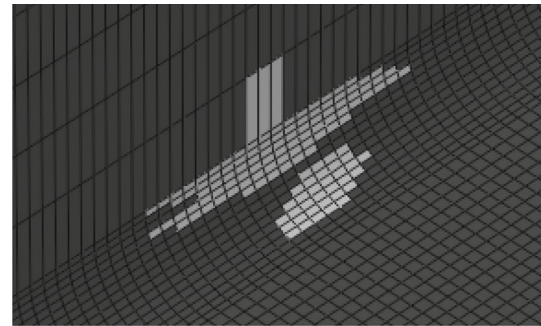


Fig. 12 The damage of the first ply in sublaminante-2

to the minimum bending of the layer. The major axis of the damage area is determined by the matrix cracking.

In general, this model can be used to understand the progressive damage of the integrated composite T-joint in aircraft structures and can be further applied to predict the delamination.

**Acknowledgements** The authors gratefully acknowledge the financial support provided by the Jiangsu Natural Science Foundation (BK20160786).

**Compliance with ethical standards**

**Conflict of interest** The authors declare that they have no conflict of interest.

**References**

1. Feng Y, Gao C, He YT et al (2016) Investigation on tension-tension fatigue performances and reliability fatigue life of T700/MTM46 composite laminates. *Compos Struct* 136:64–74

2. Degenhardt R, Castro SGP, Mariano AA, Zimmerman R, Khakimova R, Kling A (2014) Future structural stability design for composite space and airframe structures. *Thin Wall Struct* 81:29–38
3. Mandar DK, Rahul G, Naik NK (2011) Effect of back pressure on impact and compression-after-impact characteristics of composites. *Compos Struct* 93:944–951
4. Riccio A, De Luca A, Di Felice G, Caputo F (2014) Modelling the simulation of impact induced damage onset and evolution in composites. *Compos B* 66:340–347
5. Abrate S (1998) Impact on composite structures. Cambridge University Press, Cambridge
6. Rouchon J (1995) Fatigue and damage tolerance aspects for composite aircraft structures. In: Proceedings of ICAF symposium, Delft
7. Malhotra A, Guild FJ, Pavier M (2008) Edge impact to composite laminates-experiments and simulations. *J Mater Sci* 43(20):6661–6667
8. Kesavan A, John S, Herszberg I (2008) Strain-based structural health monitoring of complex composite structures. *Struct Health Monit* 7(3):203–213
9. Park H, Kong C (2013) Experimental study on barely visible impact damage and visible impact damage for repair of small aircraft composite structure. *Aerosp Sci Technol* 29:363–372
10. Zhu L, Cui H, Li Y et al (2012) Numerical simulation of the failure of composite T joints with defects. *Acta Aeronaut Astronaut Sin* 33:287–296
11. Giovanni B, Roberto V (2003) Influence of the laminate thickness in low velocity impact behavior of composite materials plate. *Compos Struct* 61:27–38
12. Cartie DDR, Irving PE (2002) Effect of resin and fiber properties on impact and compression after impact performance of CFRP. *Compos Part A* 33:483–493
13. Cantwell WJ (2007) Geometrical effects in the low velocity impact of GFRP. *Compos Sci Technol* 67:1900–1908
14. Wang SX, Wu LZ, Ma L (2010) Low-velocity impact and residual tensile strength analysis to carbon fiber composite laminates. *Mater Design* 31:118–125
15. Besant T, Davies GAO, Hitchings D (2001) Finite element modeling of low velocity impact of composite sandwich panels. *Compos Part A* 32:1189–1196
16. Yademellat Hesam, Nikbakht Ali, Saghafi Hsmed (2010) Experimental and numerical investigation of low velocity impact on electrospun nanofiber modified composite laminates. *Compos Struct* 200:507–514
17. Ma Xueshi, Bian Kan, Ji-yun Lu (2016) Experimental research on detection for interface debond of CFRP T-joints under tensile load. *Compos Struct* 158:359–368
18. Rhead AT, Marchant D, Butler R (2010) Compressive strength of composite laminates following free edge impact. *Compos A Appl Sci Manuf* 41(9):1056–1065
19. Choi HY, Chang K (1992) A model for predicting damage in graphite-epoxy laminated composites resulting from low-velocity point impact. *J Compos Mater* 26(14):2134–2169
20. Wiggenraad JFM, Zhang X, Davies GAO (1999) Impact damage prediction and failure analysis of heavily loaded, blade-stiffened composite wing panels. *Compos Struct* 45:81–103
21. Shenoi RA, Violette FLM (1990) A study of structural composite tee joints in small boats. *J Compos Mater* 24:644–665
22. Greenhalgh E, Meeks C, Clarke A, Thatcher J (2003) The effect of defects on the performance of post-buckled CFRP stringer-stiffened panels. *Compos A* 34(7):623–633
23. Greenhalgh E, Clarke A, Thatcher J (2000) Mechanical evaluation of stringer-stiffened panels tested under compression. Report: DERA.T3.TR.4. Farnborough (UK)
24. Ostre Benjamin, Bouvet Christophe (2015) Edge impact modeling on stiffened composite structures. *Compos Struct* 126:314–328
25. Faggiani A, Falzon BG (2010) Predicting low-velocity impact damage on a stiffened composite panel. *Compos A* 41:737–749
26. Greenhalgh E, Bishop SM (1996) Characterisation of impact damage in skin-stringer composite structures. *Compos Struct* 36:187–207
27. Feng Yu, Zhang Haoyu (2016) Effect of impact damage positions on the buckling and post-buckling behaviors of stiffened composite panel. *Compos Struct* 155:184–196
28. Serna Moreno MC, Lopez Cela JJ (2015) Adhesively bonded joints as a dissipative energy mechanism under impact loading. *Appl Math Model* 39:3496–3505
29. Cui Hai-Po, Wen Wei-Dong, Cui Hai-Tao (2009) An integrated method for predicting damage and residual tensile strength of composite laminates under low velocity impact. *Comput Struct* 87:456–466
30. Hua Huang Chien, Jung Lee Ya (2003) Experiments and simulation of the static contact crush of composite laminated plates. *Compos Struct* 61(3):265–270
31. Camanho PP, Davila CG (2002) Mixed-mode decohesion finite elements for the simulation of delamination in composite materials. National Aeronautics and Space Agency, USA: NASA-technical paper, pp 211737
32. Camanho PP, Matthews FL (1999) A progressive damage model for mechanically fastened joints in composite laminates. *J Compos Mater* 33:2248–2280
33. Atas A, Soutis C (2014) Strength prediction of bolted joints in CFRP composite laminates using cohesive zone elements. *Compos B Eng* 58:25–34
34. Borg R, Nilsson L (2004) Simonsson K. Simulating DCB.ENF and MMB experiments using shell elements and a cohesive zone model. *Compos Sci Technol* 64:269–278
35. Moroni F, Pirondi A (2011) Cohesive zone model simulation of fatigue debonding along interfaces. *Procedia Eng* 10:1829–1834